

DEVELOPMENT OF A HYDROSTATIC JOURNAL BEARING WITH SLIT-STEP COMPENSATION

Layton C. Hale¹, Robert R. Donaldson²,
 Carlos Castro³, Carl A. Chung³, David J. Hopkins³

¹Innovative Machine Solutions
 Dublin, CA, USA

²Independent Consultant
 Pittsboro, NC, USA

³Lawrence Livermore National Laboratory
 Livermore, CA, USA

INTRODUCTION

This paper describes the mathematical modeling and initial testing of an oil-hydrostatic bearing that derives compensation from both a central radial slit where fluid enters and stepped clearances near each end. Bearings using either a radial slit or stepped clearances for compensation were well studied over forty years ago by Donaldson [1]. These bearings have smooth bores uninterrupted with multiple recesses around the circumference. The present slit-step bearing achieves the best of both types with somewhat higher hydrostatic stiffness than the slit bearing and fluid shear drag lower than the step bearing. This is apparent in TABLE 1, which compares calculated values of initial (i.e., centered) hydrostatic stiffness for each type. The slit-step bearing is one of several types being studied at Lawrence Livermore National Laboratory for possible use on the Precision Optical Grinder and Lathe (POGAL).

TABLE 1. Hydrostatic stiffness (normalized to pressure, projected area and inverse clearance) for three types of compensation, all with length-to-diameter ratio $\frac{1}{2}$.

Type of compensation	Clearance ratio	Hydrostatic stiffness
Radial slit	-	0.55
Stepped clearance	2	0.28
Slit plus step	3	0.73

A general understanding of the different compensation schemes may be obtained by studying FIGURES 1-3. Each one shows a cross section through the upper half of the bearing with exaggerated clearances. The pressure profile along the length of the bearing is shown at nominal clearance (solid) and either side of nominal (dashed). The supply pressure is constant

and the bearing film pressure decreases to zero (atmospheric pressure) at each end. The bearing exhibits positive stiffness when the film pressure integrated over the bearing area increases as the clearance decreases.

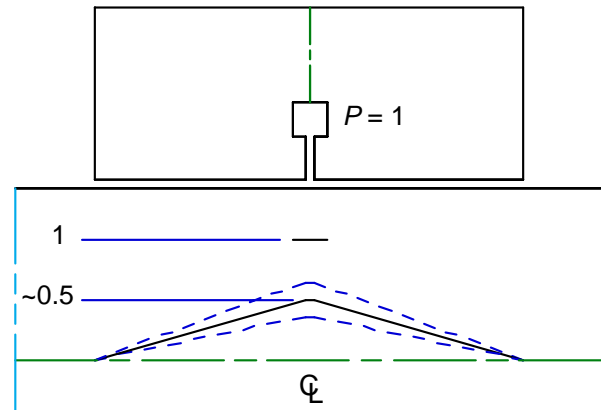


FIGURE 1. Cross section of the radial-slit bearing with the pressure profile superimposed.

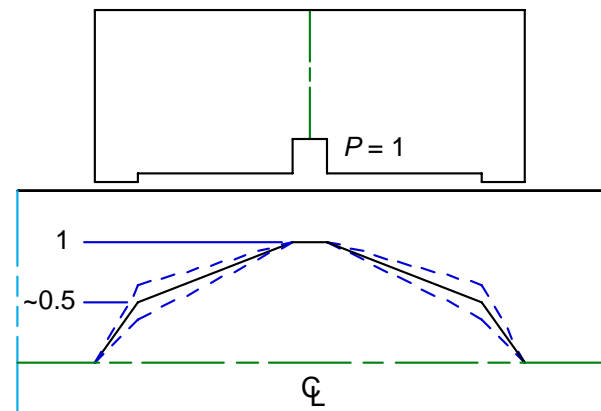


FIGURE 2. Cross section of the stepped-clearance bearing with the pressure profile superimposed.

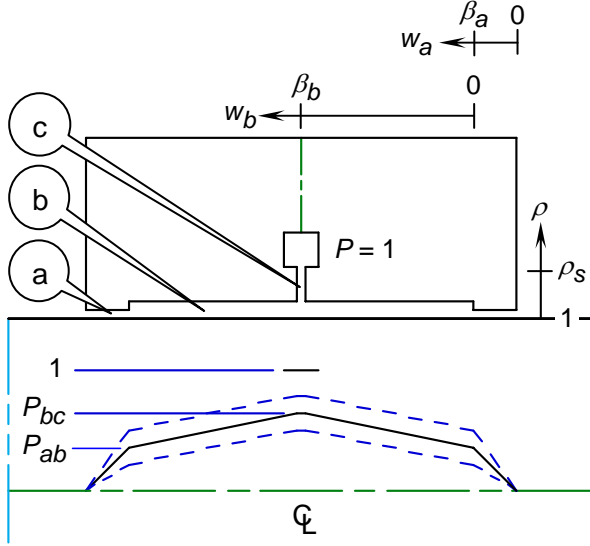


FIGURE 3. Cross section of the slit-step bearing with the pressure profile superimposed. It has three regions: (a) land, (b) recess and (c) slit.

The stiffness advantage of the slit-step bearing results from the recess distributing the pressure response from the slit over most of the bearing length. However, the recess cannot be too deep. Fluid flows circumferentially from the higher-pressure side to the lower-pressure side more significantly for a larger recess-to-land clearance ratio and a larger length-to-diameter ratio, resulting in lower stiffness. These are important parameters when optimizing the bearing for high stiffness and low heat generation.

ANALYTICAL MODEL

The approach Donaldson used to model radial-slit and stepped-clearance bearings in [1] extends readily to the slit-step bearing of interest here. It involves piecing together solutions for partial differential equations in each region by matching flow and pressure at each junction.

The model starts with the dimensionless Reynolds equation, given in (1) for hydrostatic (HS), hydrodynamic (HD) and squeeze-film (SF) modes of operation. Being linear in pressure, the complete solution may be superimposed from separate solutions found for each mode as in (2). Our nomenclature is consistent with that in [1] except for minor changes in notation. TABLE 2 lists those variables with simple normalizations. The dimensionless parameter groups Γ and Ω appearing in (2) relate characteristic HD and SF pressures to the HS supply pressure. To further clarify, the subscripts in (2) are implied in (1) corresponding to the right-hand side, since

superscripts and subscripts are needed later to identify the order and region associated with P .

$$\frac{\partial}{\partial w} \left(H^3 \frac{\partial P}{\partial w} \right) + \frac{\partial}{\partial \theta} \left(H^3 \frac{\partial P}{\partial \theta} \right) = \begin{cases} 0 & \text{HS} \\ \frac{\partial H}{\partial \theta} & \text{HD} \\ \cos \theta & \text{SF} \end{cases} \quad (1)$$

$$\frac{p}{\rho_s} = P_{HS} + \Gamma P_{HD} + \Omega P_{SF} \quad (2)$$

TABLE 2. Nomenclature

Symbol	Variable	Normalized to:
P	Pressure	Supply pressure
θ	Angle (radians)	-
ρ	Radial position	Bearing radius
w	Axial position	Bearing radius
β	Bearing length	Bearing radius
H	Film thickness	Land clearance
G	Recess clearance	Land clearance
γ	Slit gap	Land clearance
ε	Eccentricity	Land clearance

Reynolds equation is accurate under the following conditions: incompressible, Newtonian fluid with constant viscosity, viscous-dominated flow, and very small clearances compared to the other length scales. In addition, the bearing surfaces are assumed to be perfectly aligned and free from deformations and form errors.

To facilitate solutions for (1), the pressure distribution is represented in (3) as a perturbation expansion in eccentricity ε . Terms up to first order are sufficient for HS and HD equations, while zero-order terms are sufficient for SF equations. This small- ε approximation will have error of order ε^2 .

$$P(w, \theta) = P^{(0)} + \varepsilon \cdot P^{(1)} \quad (3)$$

The film thickness H is constant in w for each region and has θ dependence as described in (4) for the land and recess regions, respectively.

$$\begin{aligned} H_a(\theta) &= 1 + \varepsilon \cdot \cos \theta \\ H_b(\theta) &= G + \varepsilon \cdot \cos \theta \end{aligned} \quad (4)$$

Substituting (3) and (4) into (1) yields a mix of zero-, first- and higher-order terms in ε . The higher-order terms of course are discarded and like terms are collected into separate equations, (5) and (6), each of which must be satisfied. Written for the recess region, these equations also apply to the land region by setting $G = 1$.

$$\frac{\partial^2 P^{(0)}}{\partial w^2} + \frac{\partial^2 P^{(0)}}{\partial \theta^2} = G^{-3} \begin{cases} 0 & \text{HS} \\ 0 & \text{HD} \\ \cos \theta & \text{SF} \end{cases} \quad (5)$$

$$\frac{\partial^2 P^{(1)}}{\partial w^2} + \frac{\partial^2 P^{(1)}}{\partial \theta^2} = G^{-3} \begin{cases} 0 & \text{HS} \\ -\sin \theta & \text{HD} \end{cases} \quad (6)$$

The slit region has uniform and constant gap so the polar-coordinate form of the Laplace equation (7) holds for both zero- and first-order pressure terms.

$$\frac{\partial}{\partial \rho} \left(\rho \frac{\partial P}{\partial \rho} \right) + \frac{\partial^2 P}{\partial \theta^2} = 0 \quad (7)$$

It is worth making some observations at this point to save work downstream. In the centered position ($\varepsilon = 0$), the hydrostatic pressure distribution lacks θ dependence in any of the three regions. The pressure distribution that solves the HS term in (5) is linear along the axis, as pictured in FIGURE 3. In the slit, a logarithmic pressure distribution solves (7) for the centered position.

A centered hydrodynamic bearing does not generate pressure so only the first-order HD pressure is nonzero. As noted earlier, only the zero-order SF pressure is needed for small eccentricity. Upon examining the HD term in (6) and the SF term in (5), they differ only in the forcing function on the right side, $\cos \theta$ vs. $-\sin \theta$. In both cases, the pressure distribution is generated by lateral velocity, so we should expect both solutions to be identical except for a 90° phase difference in θ . Thus only one solution need be carried further, and there is some utility in addressing the terms in (6), i.e., HS and HD.

Returning to the zero-order hydrostatic pressure, the two junction pressures along with known boundary pressures completely determine the distribution. We could choose to specify them as design parameters or calculate them from specified physical parameters. Since both slit and step bearings have only one junction, it is typical to specify the junction pressure at 0.5, the optimal value. The slit-step bearing does not have a tidy optimum so our preference is to calculate the junction pressures from physical parameters. Matching flow rates across two junctions gives two equations in (8) to solve for the two unknown junction pressures in (9).

$$\frac{1}{\beta_a} P_{ab} = \frac{G^3}{\beta_b} (P_{bc} - P_{ab}) = \frac{\gamma^3}{2 \ln \rho_s} (1 - P_{bc}) \quad (8)$$

$$\begin{bmatrix} P_{ab} \\ P_{bc} \end{bmatrix} = \frac{1}{\beta_a + G^{-3} \beta_b + 2\gamma^{-3} \ln \rho_s} \begin{bmatrix} \beta_a \\ \beta_a + G^{-3} \beta_b \end{bmatrix} \quad (9)$$

Now the boundary conditions can be determined for the first-order pressure distributions. The three regions require a total of six equations and most are functions of θ . Two are externally imposed pressures, and the remaining four come from pressure and flow matching at the two junctions. Without further explanation, they appear in (10) through (15).

$$P_a^{(1)}(0, \theta) = 0 \quad (10)$$

$$P_a^{(1)}(\beta_a, \theta) = P_b^{(1)}(0, \theta) \quad (11)$$

$$P_b^{(1)}(\beta_b, \theta) = P_c^{(1)}(1, \theta) \quad (12)$$

$$P_c^{(1)}(\rho_s, \theta) = 0 \quad (13)$$

$$\left. \frac{\partial P_a^{(1)}}{\partial w_a} \right|_{\beta_a} - G^3 \left. \frac{\partial P_b^{(1)}}{\partial w_b} \right|_0 = -3 \frac{G-1}{G} \cos \theta \begin{cases} P_{ab} \beta_a^{-1} \\ 0 \end{cases} \quad (14)$$

$$G^3 \left. \frac{\partial P_b^{(1)}}{\partial w_b} \right|_{\beta_b} - \frac{\gamma^3}{2} \left. \frac{\partial P_c^{(1)}}{\partial \rho} \right|_1 = -\frac{3}{G} \cos \theta \begin{cases} P_{ab} \beta_a^{-1} \\ 0 \end{cases} \quad (15)$$

The general solution to (6) and the applicable boundary equations is given in (16), where A_i , B_i and C_i are constants to be determined for regions (a) and (b). Likewise, the general solution to (7) for region (c) is given in (17).

$$P_i^{(1)}(w_i, \theta) = (A_i \sinh w_i + B_i \cosh w_i + C_i) \begin{cases} \cos \theta \\ -\sin \theta \end{cases} \quad (16)$$

$$P_c^{(1)}(\rho, \theta) = \left(A_c \rho + \frac{B_c}{\rho} \right) \begin{cases} \cos \theta \\ -\sin \theta \end{cases} \quad (17)$$

Next the solutions are substituted into the differential equations and boundary equations to determine the constants. Several constants are easily found and the remaining four are represented in a matrix equation (18) to facilitate their simultaneous solution and to easily compute the HS and HD stiffness in (19). Being nondimensional with the same normalization used in [1], it is satisfying to find numerical agreement with the two limiting cases that can be cross checked, i.e., radial-slit and stepped-clearance bearings.

$$\underbrace{\begin{bmatrix} \sinh \beta_a & 0 & -1 & 0 \\ 0 & \sinh \beta_b & \cosh \beta_b & -(\rho_s^2 - 1) \\ \cosh \beta_a & -G^3 & 0 & 0 \\ 0 & G^3 \cosh \beta_b & G^3 \sinh \beta_b & \frac{\gamma^3}{2}(\rho_s^2 + 1) \end{bmatrix}}_{\mathbf{M}} \begin{bmatrix} A_a \\ A_b \\ B_b \\ A_c \end{bmatrix} = \begin{cases} \mathbf{b}_{HS} \\ \mathbf{b}_{HD} \end{cases} = \begin{bmatrix} 0 \\ 0 \\ 1-G^{-1} \\ G^{-1} \end{bmatrix} \begin{bmatrix} 3 \\ \beta_a + G^{-3} \beta_b + 2 \gamma^{-3} \ln \rho_s \\ 1-G^{-3} - \cosh \beta_a \\ G^{-3} \\ -\sinh \beta_a \\ 0 \end{bmatrix} \quad (18)$$

$$\begin{cases} K_{HS} \\ K_{HD} \end{cases} = \frac{\pi}{2(\beta_a + \beta_b)} \begin{cases} \mathbf{a} \cdot \mathbf{M}^{-1} \cdot \mathbf{b}_{HS} \\ \beta_a + G^{-3} \beta_b - \sinh \beta_a - \mathbf{a} \cdot \mathbf{M}^{-1} \cdot \mathbf{b}_{HD} \end{cases} \quad (19)$$

$$\mathbf{a} = [\cosh \beta_a - 1 \quad \cosh \beta_b - 1 \quad \sinh \beta_b \quad 0]$$

Turning (19) into a dimensional form requires: the supply pressure p_s , the land clearance c_a , the bearing length L and diameter D , and the dimensionless parameter groups Γ and Ω from (2). Both Γ and Ω include the fluid viscosity μ and a characteristic velocity, which can be chosen to yield a common expression. For the HD stiffness, it is the bulk circulation frequency of the fluid at one-half the shaft speed. For the SF stiffness, it is the excitation frequency. It is convenient to express the bearing stiffness (20) as a complex number, with the real HS stiffness and the imaginary stiffness that is 90° out of phase either in space (HD) or in time (SF).

$$k(\omega) = p_s L \frac{D}{c_a} K_{HS} + (i\omega) 3 \mu L \left(\frac{D}{c_a} \right)^3 K_{HD} \quad (20)$$

TEST SPINDLE

A test spindle was built with less than \$500 capital investment in materials, in particular, ground-and-polished steel stock for the rotor and SAE 660 bronze bar for the journals. Other materials were found on site, and a variable-speed router motor provides an inexpensive drive solution. The authors constructed the test spindle on site. The journals and housing were turned on a Hardinge tool-room lathe and aligned concentric to one another on a Moore No. # 3 Measuring Machine.

INITIAL TEST RESULTS

The static compliance of the spindle was measured midway between the bearings by applying a force to the shaft with a force gauge and measuring the displacement of the shaft with respect to the housing using a capacitance gauge. The shear plus bending compliance of the shaft is reliably calculated to be 2.1 nm/N. Subtracting this from the total measured compliance and ignoring the compliance in the housing, the compliance for each bearing is 16 nm/N, or in terms of stiffness, 61 N/μm. The calculated stiffness using the nominal design parameters and the supply pressure of the test, 1.3 MPa, is somewhat larger at 77 N/μm. This discrepancy could result from a number of sources but we suspect larger-than-intended clearance.

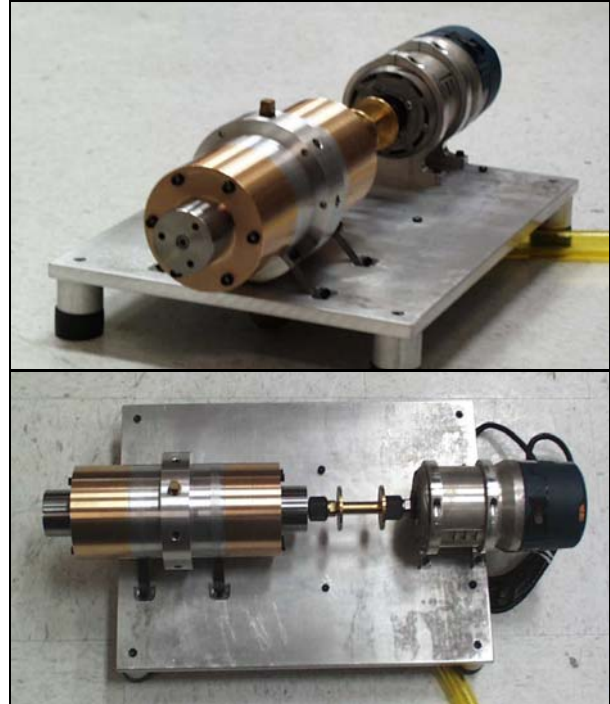


FIGURE 4. Two views of the test spindle.

ACKNOWLEDGEMENTS

This work was performed under the auspices of the U.S. Department of Energy by the Lawrence Livermore National Laboratory under Contract No. W-7405-ENG-48.

REFERENCES

1. Donaldson, R.R., June 1965, *Incompressible Journal Bearings with Combined Hydrostatic-Hydrodynamic Action*, Ph.D. Thesis, Massachusetts Institute of Technology.